Spring 5-2021

A Method for Orientation of Cellulose Nano Fibers for Addition of Biological Nanoparticles and Tissue Integration

Joshua Hamilton

A METHOD FOR ORIENTATION OF CELLULOSE NANO FIBERS FOR ADDITION OF BIOLOGICAL NANOPARTICLES AND TISSUE INTEGRATION

by

Joshua Hamilton

A Thesis Submitted in Partial Fulfillment
of the Requirements for a Degree with Honors
(Biomedical Engineering)

The Honors College

University of Maine

May 2021

Advisory Committee:

Karissa Tilbury, Assistant Professor of Biomedical Engineering, Advisor
Michael Mason, Professor of Biomedical Engineering
Andre Khalil, Professor of Biomedical Engineering
Scott Collins, Professor of Chemistry
Melissa Ladenheim, Associate Dean of Honors College

ABSTRACT

The University of Maine is one of the world's leading producers of cellulose nanofibers (CNF). This material has the power to revitalize the Maine paper industry. This has led to an abundance of labs on campus researching applications for the material. Active research activities at the University of Maine include industrial applications such as, filtration, biodegradable packaging, building materials and niche health care applications. Niche health care applications include wicking pads for point of care diagnostics and tunable biomaterials ranging from dressings to implantable bone-like materials. Medical applications require an analysis of the biocompatibility of CNF. CNF is biocompatible in general: however, the degree of biocompatibility, particularly for tissue engineering applications involving long term integration within the body, is an area of active research. CNF is a highly tunable biomaterial; control of the fibril anisotropy dramatically alters bulk biomechanical properties which also modulates biological interaction. To tune fiber anisotropy, a novel strategy to produce single direction-oriented CNF films by application of a unilateral force via a latex substrate was developed. The alignment of CNF films was characterized using both polarized light microscopy and scanning electron microscopy (SEM). CNF is birefringent; therefore, using polarized light microscopy the alignment of CNF can be inferred by quantifying the birefringence optical index (BOI). The BOI ranges from -1 to 1, with high birefringence found at the extrema values. To validate the birefringence orientation sensitivity to CNF film alignment; we performed SEM for direct assessment of fiber alignment using OrientationJ, a FIJI plugin. Hydroxyapatite (HA) was incorporated as an additive to evaluate the application of this method to cellulose nano composites. Both the BOI and

the SEM fibril analysis confirmed that CNF fibrils are aligned preferentially along the axis of force transmission. Furthermore, the addition of HA did not diminish the degree of CNF fibril alignment. Overall, we demonstrate a rapid and economic approach to fabricate and assess fibril alignment in CNF films useful for a myriad of tissue engineering applications.

ACKNOWLEDGEMENTS

I would like to take this time to acknowledge the opportunity granted to me by the Center of Undergraduate Research in funding the portion of this research performed over the summer. This gave me a great distraction from the pandemic and helped with my mental health by giving me something positive to apply myself too.

I would like to thank Prof. Tilbury and Prof. Mason for guiding me throughout this research and offering me their sage advice, as well as being some of the only people I saw throughout the summer. I would like to thank Prof. Khalil for his tips about image analysis and recommendations for histograms and participation in my committee. I would also like to thank Prof. Collins for his suggestions about possible nanoparticle orientation methods and for his positive participation throughout the course of this research. Sahar Roozabahani, a graduate student, also deserves thanks for her multitude of contributions to the project.

I would like to thank Prof. Ladenheim for her constant support and assistance. She spent an unknown amount of time reading through and critically analyzing the many drafts of my 14-page reading list, resulting in a product I am extremely proud of.

Lastly, I would like to thank my Mom, Shelly Spear-Hamilton, for all the work and suffering she has put herself through in order to keep a roof over our heads despite divorce and loss. Without her, I would not have the ability to even attend the University of Maine and have the time to complete this research and other opportunities throughout my life.

TABLE OF CONTENTS

LIST OF FIGURES AND TABLES

CHAPTER 1: INTRODUCTION

Scientists predict that we have already entered irreversible climate change or have less than 10 years to fix our climate [1]. This is a problem that requires creative, material engineering solutions in order to migrate from nonrenewable materials to renewable. One type of nonrenewable material that needs a replacement are oil derived polymers such as plastics. Over 300 million tons of plastic are produced annually which ultimately reaches our dumps and our oceans [1]. Biodegradable plastic replacements fall under a material class known as biopolymers which includes cellulose. Cellulose is the most abundant organic compound in the world and is the raw material in paper [2]. Pulp, the processed form of cellulose in papermaking once further refined under high pressure mechanical grinding produces a cellulose product with nanometer features known as cellulose nanofibers (CNF) [3].

The University of Maine is the world's largest processor of CNF; a vital asset to revitalize Maine's pulp and paper industry which was once the largest in the United States with 25 paper mills [4,5]. Cellulose nanofibers (CNF) have several sought-after material properties as a biologically derived polymer including “crystallinity, high specific surface area, rheological properties, liquid crystalline behavior, alignment and orientation, mechanical reinforcement, barrier properties, surface chemical reactivity, biocompatibility, biodegradability, and lack of toxicity” [6]. These properties have led researchers across the world and across the University of Maine to study diverse industrial applications of the material such as, 3d printing, food packaging, and air filtration [7, 8, 9]. Perhaps more exciting are the niche medical applications which utilize CNF’s biocompatibility and biodegradability. These applications utilize CNF as a substrate to

encourage cell growth and repair, due to its strength and ability to offer subcellular scale attachment sites. Tissue engineering for incorporation of CNF into longer term body implants is an active area of research at the University of Maine.

Multiple professors within the Chemical and Biomedical Engineering department at the University of Maine are at the forefront of these niche medical applications. Dr. Michael D. Mason is researching CNF as a possible bone screw/implant replacement and Dr. David J. Neivandt is researching using CNF as a nerve repair conduit. A key criteria of biomedical engineering device design is the control of tissue integration for proper function. For example, **Figure 1** is a mechanical heart valve. The suture ring requires cellular ingrowth; whereas the valve leaflets must lack cellular integration to ensure proper

Figure 1: Commercial Heart Valve by CryoLife. Reproduced from Ref. [10]

function during every single heartbeat. While cell integration and viability are dependent of the material itself, CNF offers a way to manipulate other facets known to affect cells such as fibril length, width, curvature, mechanical force, and orientation [11]. These 3d organizational structure cues affect extra cellular matrix (ECM) organization and communication between cells, so to create proper replacement tissue matrices, fine control of these structural properties will be necessary. For example, a paper in the Journal of Biomaterials studied another biodegradable polymer, polylactic-co-glycolic acid (PLGA),

and discovered that cell spreading, and aspect ratio of cells increased "systematically with increasing fiber orientation" [12]. An earlier published paper confirms this same relationship and even found increasing cell densities for smooth muscle cells on increased PLGA fiber orientations [13]. Intuitively, the effect of orientation can be seen in **Figure 2** which are scanning electron microscopy (SEM) images of cell movement on microfabricated nanostructured substrates. The cell can be seen moving along the oriented groove. CNF are at a slightly smaller scale than the grooves in **Figure 2,** as the ones produced at the

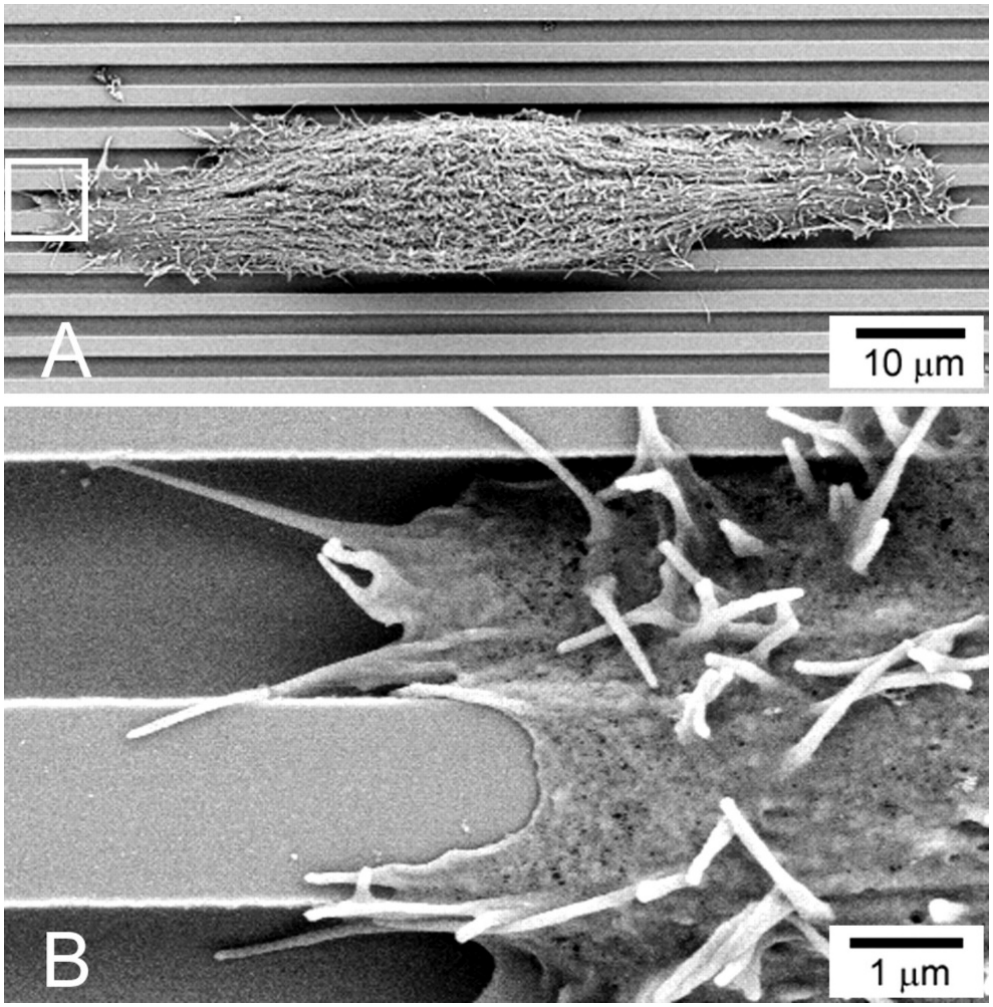

Figure 2: Cell Movement on Nanofabricated Grooves. Reproduced from Ref [14]

University of Maine are 20-50 nm in width and hundreds of microns in length. This difference in scale requires active research to determine if cells will experience similar effects to the smaller CNF attachment sites or if nanofiber bundling will be the dominant supporting structure for cells. This requires the ability to produce oriented CNF films for studying cell behavior on CNF. CNF also offers the ability to tune many other structural factors than shown in **Figure 2,** such as curvature or tension similar to the PLGA studies.

While PLGA has a multitude of studies into understanding its structural effects on cells as a material for niche medical applications, it suffers from many disadvantages in comparison to CNF. A major research area for biopolymers is bone replacement, of which

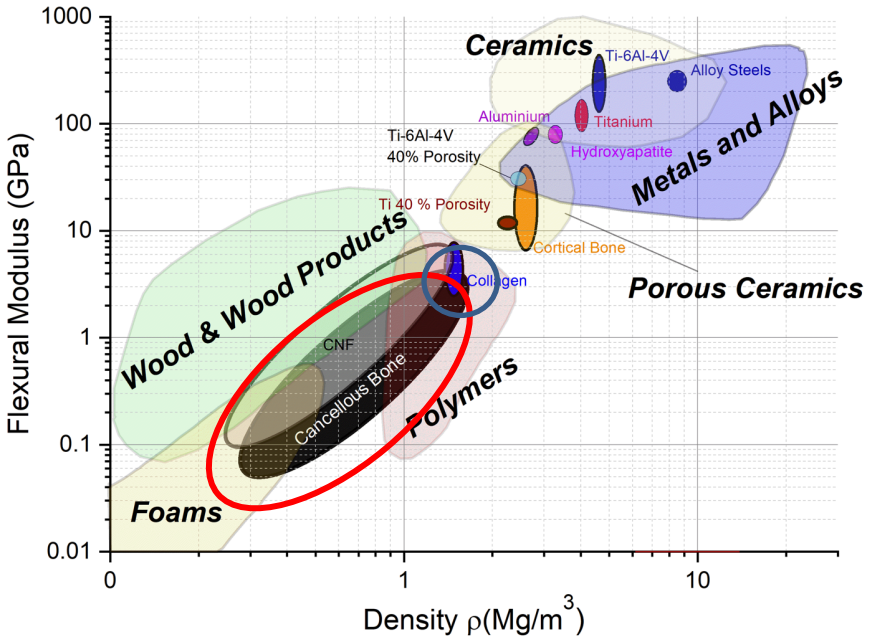

Figure 3: Ashby Plot of Multiple Material's Density vs Flexural Modulus, CNF is Found Near Bone and Wood Products in the Red Highlighted Area, PLGA in Blue Area

CNF is the superior biopolymer for this application, which can be seen in **Figure 3**, an Ashby plot demonstrating how CNF's flexural modulus and density is similar to bone.

PLGA has both a lower tensile strength and a lower young's modulus than CNF while CNF's material properties are highly tunable through anisotropic modifications [15]. For example, this tunability could become a key factor in preventing stress shielding of bone implants. Randomly oriented CNF can have a tensile strength upwards of 6 GPa which is similar to steel [15]. With oriented fibril structures the longitudinal axis can reach upwards of 100 GPa with a compressive strength of 16 GPa [15]. This gives a huge range of possible tensile strengths allowing the same material to be used in different applications by controlling orientation. Cells can also sense the mechanical properties of the substrate they are in and therefore tissue integrating implants must successfully replicate the extra cellular matrix of the tissue. The tunability of CNF mechanical properties then should lead to the tunability of cellular integration alongside the mentioned effects of fiber orientation on cells. This leads CNF to serve as a great substrate for high strain tissue replacement such as bone or tendons, or due to its hydrophilicity, any biological replacement where you want the body to slowly reclaim the area.

To create successful applications of CNF, the tunability of mechanical properties and fiber structure must be controlled in order to then understand and quantify their effects on cells. CNF films serve as a good starting point for this research avenue due to their ease of imaging and removal of macro 3d effects. Once the film structure and property relationship to cell proliferation and integration is understood, non-film material tuning can begin. The first goal for this research avenue is to effectively quantify and produce oriented dried CNF films to determine what drying methodologies will produce films that cells will find attractive. To further increase the range of tunability and material applications this drying methodology should work regardless of nanoparticle additions. For example, this would allow the addition of hydroxyapatite (HA) nanoparticles which are known to

encourage bone integration with grafts and implants [16]. To determine fibril orientation, imaging methods will be needed in order to quantitatively study and compare drying methodologies.

CHAPTER 2: ORIENTATION METHODOLOGIES

There are various methods to align biopolymer films, such as CNF, which include application of electromagnetic fields (EM Field) or mechanical forces to biopolymer films. Various methodologies reviewed from the literature or applied during this thesis research will be discussed throughout this chapter, including the final developed methodology for this thesis.

2.1: Vacuum Filtration

This method, developed at the University of Maine, is from the literature and involves a basic Organic Chemistry filter paper vacuum filtration set up [15]. First, 10 mL of 1% CNF slurry is spread across filter paper. For oriented films, the filter paper is placed onto the vacuum filtration setup for 5 minutes. After 5 minutes it is removed from the vacuum filtration setup and left to dry for 5 more minutes. After the drying period, using a scoopula, 2 cm width rectangles are cut along the CNF, but not through the filter paper. These rectangular CNF pieces are carefully peeled from the filter paper and then placed onto the lab counter. The smaller width sides are then taped down and left to dry out overnight. For unoriented films the filter paper is never placed onto the vacuum and the CNF slurry is left to dry on the filter paper.

2.2: Hanging and Machine Stretched Rubber Substrate Drying

This method was developed using ideas from polymer film chemistry and a brainstorming session involving Dr. Karissa Tilbury, Dr. Michael Mason, and Joshua Hamilton. A thin

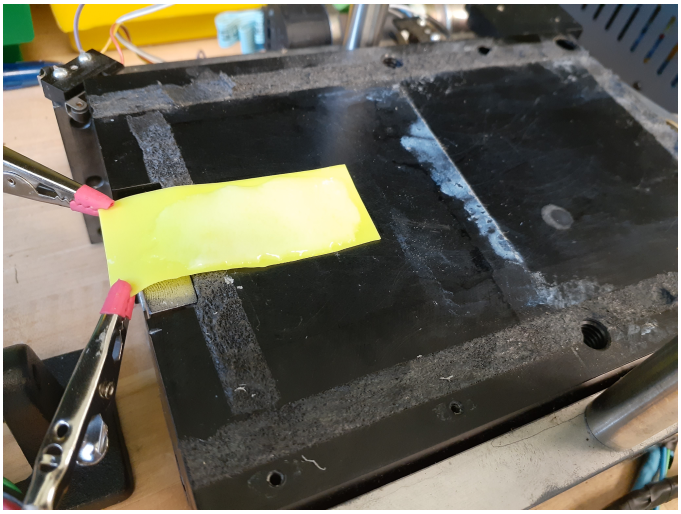

Figure 4: After Applying CNF to Rubber Substrate

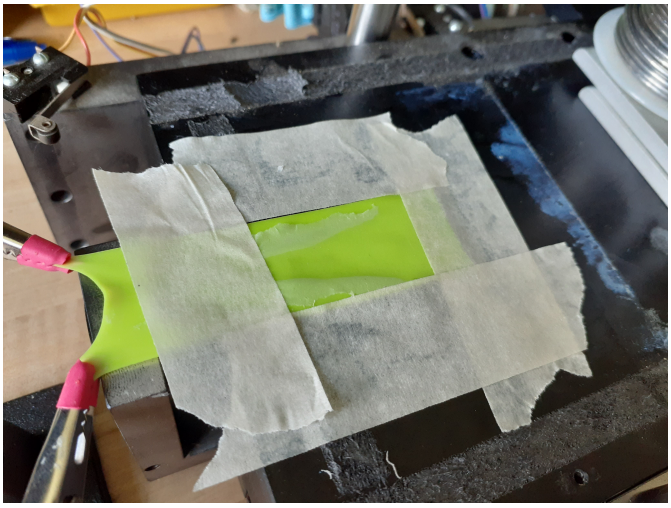

Figure 5: During Stretching of CNF Using Machine Drying Apparatus

stretchable rubber substrate was obtained and cut into 2 cm by 9 cm rectangles. 6 grams of 1 % CNF slurry is applied to one of the 2 cm width ends. Using a scoopula, the slurry was slid across the surface leaving a thin layer of CNF with the excess slurry being removed

and disposed of. For unoriented films the CNF is left to dry on the substrate. For oriented films after 3 hours of drying the substrate was then hung vertically with a 30 g weight attached to the end and left for a 24-hour period. **Figure 4** and **Figure 5** show the two steps involved in producing these films. **Figure 4** is after spreading the film and if non stretched would be left at this step, where **Figure 5** shows the machine stretching. This methodology was replaced by the final methodology described below due to uneven stretching and lack of force control. The uneven stretching can be seen in **Figure 5** where the CNF is peeling off the substrate near the edges.

2.3: Final Developed Methodology

Based on the success of the earlier, machine stretched, methodology (Ch. 4.1 for results) a new methodology was developed to accurately control the force the sample receives. For this methodology, three groups of films were made. The first group of samples referred to as “unstretched” samples were made by diluting CNF at 3wt % solid content to 1.5% to achieve a solution with lower viscosity which is easier to spread. Then, a thin, 6 g layer of the solution was spread on a rectangular 2 by 5 cm cut of latex band and taped at the edges to avoid dripping, but not on the CNF itself. Samples were left at room temperature overnight to dry. The second group of samples referred to as “stretched pure CNF” films were made by uniformly distributing a thin, 6 g layer of 1.5% CNF suspension onto the rubber latex band with the edges being taped. Then, they were placed in a confined container with controlled air flow to decrease their moisture content by 30% (3 hours of drying). At this stage, the latex band was stretched vertically by applying a force to one end while the other end was fixed and left to dry at room temperature overnight. The CNF solution adheres to the rubber latex band after 3 hours of drying at room temperature,

therefore, when the band is stretched the thin layer of CNF suspension attached to the band will become stretched as well. These steps can be seen in **Figure 6**, and this setup is covered by a box when drying to minimize effects of changing airflows.

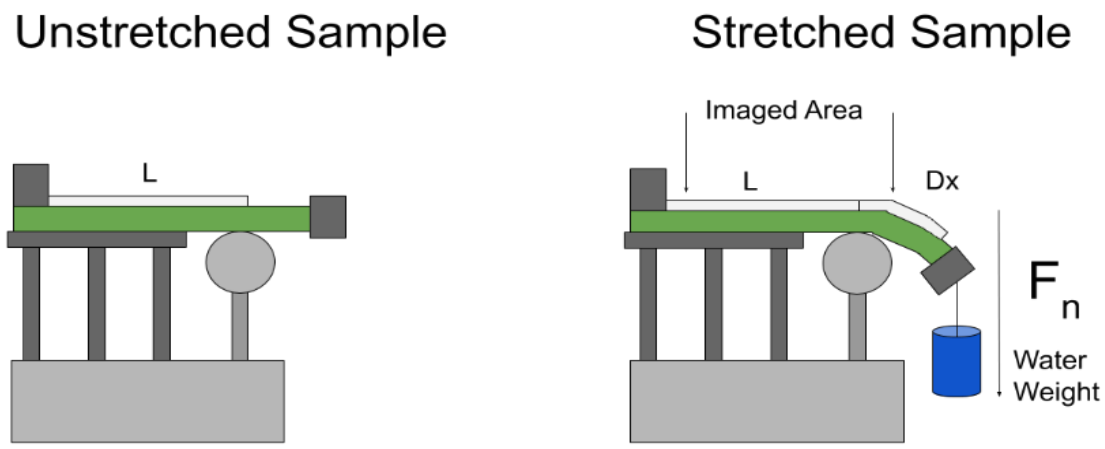

Figure 6: Schematic of Final Methodology Developed for CNF Film Stretching

The third group was developed to demonstrate the ability of this methodology to handle nanoparticulate additions to the suspension without affecting film orientation. In this case hydroxyapatite (HA) was chosen, as up to 70% of natural bone consists of hydroxyapatite and it will improve the bioavailability of the host material such as bone implants for future applications of this material [17]. The suspension used in this methodology was 90% CNF and 10% HA by dried mass. The third group referred to as "CNF/HA" were produced by adding HA powder to the 1.5% CNF suspension, and the solution was stirred at 200 rpm for 4 hours to disperse the HA into the CNF network. After 4 hours, a thin layer of CNF/HA solution was uniformly distributed on the latex band. They were taped on the edges as before and left in a confined container with controlled air flow to decrease their moisture content by 30%. The partially dried sample was stretched vertically by applying a force to one end while the other end was fixed. The sample was

left to dry at room temperature overnight. Dried films were carefully peeled off from the latex and stored in a dry place for characterization. This methodology aside from creating the CNF/HA suspension follows the same procedure as for pure CNF stretched samples.

2.4: Advantages Over Electromagnetic Field and Hydrodynamic Methodologies

Another methodology developed in the literature involved using EM fields, taking advantage of the electromagnetic dipoles inherent to cellulose due to its atomic molecular structure. The authors of this method also recognized in order to optimize CNF film strengths; effective orientation methods are needed [18]. They take advantage of CNF fibrils having more hydrogen bonding sites than larger micrometer scale cellulose from wood fibers. They discovered the same negative electromagnetic anisotropicity used in our birefringence imaging causes a long axis perpendicular orientation in CNF suspension to a magnetic field. They found a 20% improvement in CNF film orientation using wide angle X-Ray Scattering data and SEM images of films which resulted in a doubling of CNF young's modulus, tensile strength, toughness, and yield strength. Our methodology has a major advantage over EM field orientation technologies. There are limitations in what materials can be added to the CNF suspensions. If the nanoparticle additive also has a dipole it could be oriented in different ways than the CNF, without control, as the EM fields must be specifically oriented for CNF orientation. This material addition limitation is not present in the substrate drying methodology. Also, they found a 20% increase in orientation, whereas the final developed substrate methodology demonstrates a superior orientating effect shown in the results section (Ch. 4.2 and 4.3). One advantage of EM field drying methodology is the possibility of orthogonally orienting a positive magnetic

anisotropic material or parallel orienting a negative material with respect to CNF orientation.

A unique methodology found in the literature involved application of hydrodynamic forces to electrostatically charged CNF [19]. They used a “double-flow focusing” system that squeezed the CNF from both sides. First, CNF flows down a channel and a channel running perpendicular on each side of the CNF channel slams deionized water into the CNF channel. Farther down the channel path, a similar perpendicular channel on each side does the same, but with a low PH acid. This resulted in highly oriented CNF bundles. Again, the main issue with this methodology is through the addition and dispersion of nanoparticles to modify CNF properties. If the nanoparticles are dispersed beforehand into the initial CNF slurry, they will experience different electrostatic forces than the fibrils and may even be repulsed by the nanorod fibril bundle forming in the center flow or disrupt it from forming. The authors did not test any addition of nanoparticles to this methodology. This method can only produce orientated rods for applications as a nanoscale building block material or replacement of macroscale fibers. This indicates the latex substrate unilateral force drying methodology, developed in this research, fills a gap present within CNF orienting methodologies by maintaining freedom of nanoparticle addition and CNF shape to produce biocomposites.

CHAPTER 3: IMAGING METHODOLOGIES

3.1: Birefringence orientation index (BOI) measurement

The main imaging methodology used for CNF orientation analysis was the Birefringence Orientation Index (BOI). Birefringence is based on the property that some materials can be optically anisotropic, meaning that light can experience different refractive indices depending on the direction which it travels through the material. Generally, there are two types of birefringence that occur in materials. Some materials are intrinsically birefringent which originates from the molecular structure of the material being an anisotropic crystalline structure. On the other hand, extrinsic birefringence happens as a result of the macro arrangement of molecules, such as polymer arrangement like in CNF [20].

CNF is a known birefringent material which means when it is hit by a linearly polarized light ray, two different linearly polarized rays leave the material with orthogonal polarization known as the ordinary and extraordinary rays. The ordinary ray follows Snell's law and hence is called ordinary, whereas the extraordinary ray is dependent on the axis or axes of anisotropicity of the material caused by the organized electrical environment and experiences a "speed" change. [22, 22]. The frequency (*f*) of light is maintained during this process as well as the speed of the light (*c*), shown in **Equation 1**,

$$\mathrm{f} = \frac{c}{\lambda} \quad (1)$$

therefore, the “speed” change appears as a change in wavelength (λ) which is a change in color. One ray is the fast ray, and the other is the slow ray which is dependent on how the material is changing the refractive index of the extraordinary ray. This change in color is a measure of retardation between the two rays and directly relates to the anisotropicity of the material. Isotropic CNF will randomly shift the extraordinary ray whereas orientated CNF

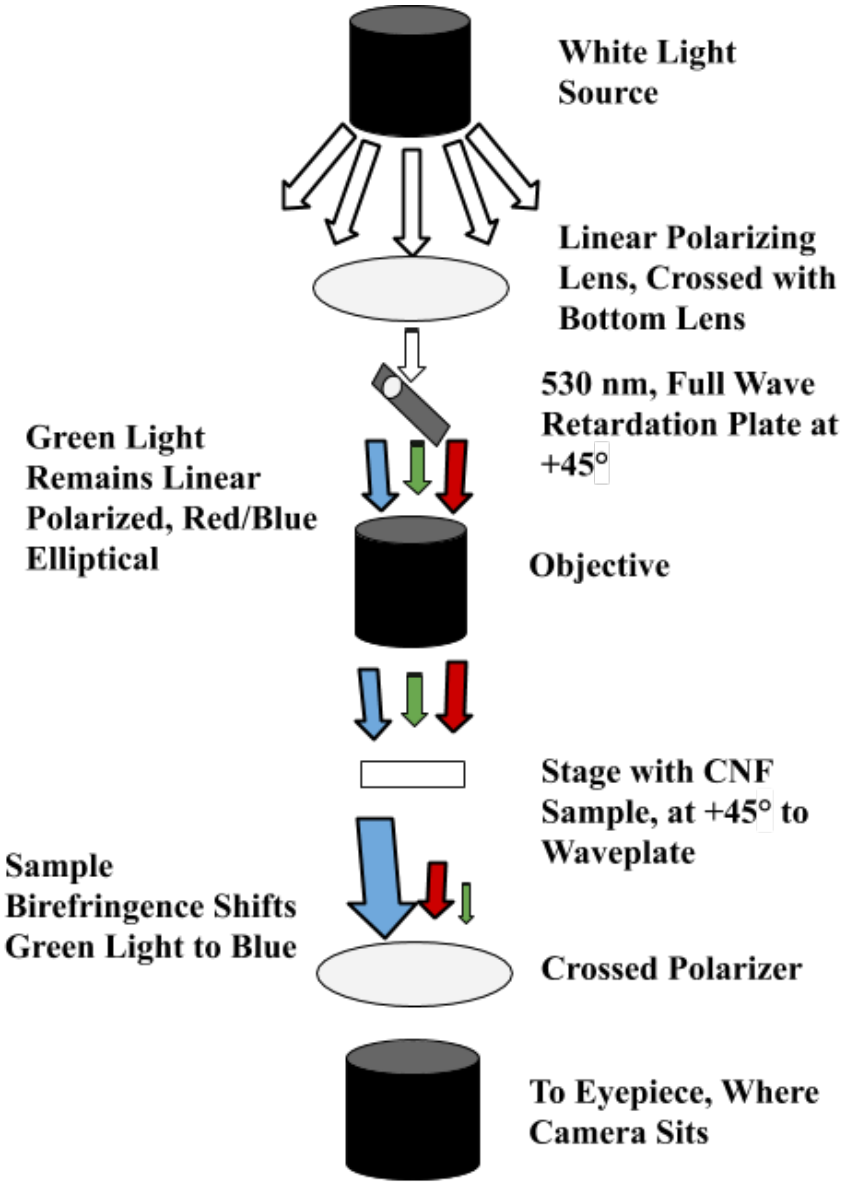

Figure 7: Schematic of Polarized Light Microscopy Setup for Birefringent Imaging

will cause a similar and repeated color shift between the two rays. The value of CNF birefringence increases with the alignment of fibers, meaning that a highly oriented film of CNF has a larger BOI compared to randomly oriented samples [22]. This BOI can be calculated using the change in color of the extraordinary ray.

To calculate the BOI a polarized light microscopy setup is being used and the path of light is shown in **Figure 7**. In a normal inverted biological microscope (Olympus IX73), two linear polarizers were added and are crossed above and below the sample stage thereby eliminating all light. Since CNF is extrinsically weakly birefringent a 530 nm full wave retardation plate is inserted at -45° angle from the center of the microscope to exaggerate wavelength shifts. This plate slows down green light leaving it linearly polarized and it elliptically polarizes red and blue light. When viewed, this means a magenta color is shown, which is a lack of green light as it is still being eliminated from the crossed polarizers. The CNF sample is then placed onto the stage and different areas of the sample are imaged. The addition of the sample causes the light to be rotated again due to CNF fibril orientation thereby allowing green light to pass through the polarizer and sometimes eliminating blue or red light. The CNF is imaged at -45° (same as wave plate) and +45° (orthogonal to waveplate). If at -45° the CNF images are yellow/red, then the CNF is retarding the green light, which is also being retarded again by the waveplate causing a greater difference between the extraordinary and ordinary ray. This is known as the fast axis [24] due to the greater difference in wavelength. When rotated to the +45° the CNF will cause an opposite change thereby decreasing retardation showing shades of blue and is called the slow axis. An unoriented sample would not display a color change and have a BOI near zero. Since the CNF goes from blue to red, from +45° to -45°, it is known as a negative birefringent material. The opposite color change would be positive birefringence. This change in blue

channel intensity can be used to determine the BOI value by **Equation 2** where *b* is the pixel intensity value in the blue channel of the RBG camera used to acquire the images. [15, 25]. Highly orientated samples will end up with values close to 1 or -1.

$$\text{BOI}=\frac{[(b_{-45})-(b_{+45})]}{[(b_{-45})+(b_{+45})]} \qquad (2)$$

The image analysis process is shown in **Figure 8** which first involves dividing the RGB (red, green, blue) image into its respective color channels. Then, the blue channel images from both angles were used to create the BOI image. The zero intensity values of the blue channels were removed by shifting the 8-bit image from 0–255 to 1–256 [26]. Furthermore, the green channel was used to create a mask and applied to the BOI image to remove noisy pixels [15]. Finally, a 1-pixel radius median filter was applied to the BOI image to smooth the map. The BOI map and histograms shown in results called **Figures 13-16** were created by this described method using FIJI software.

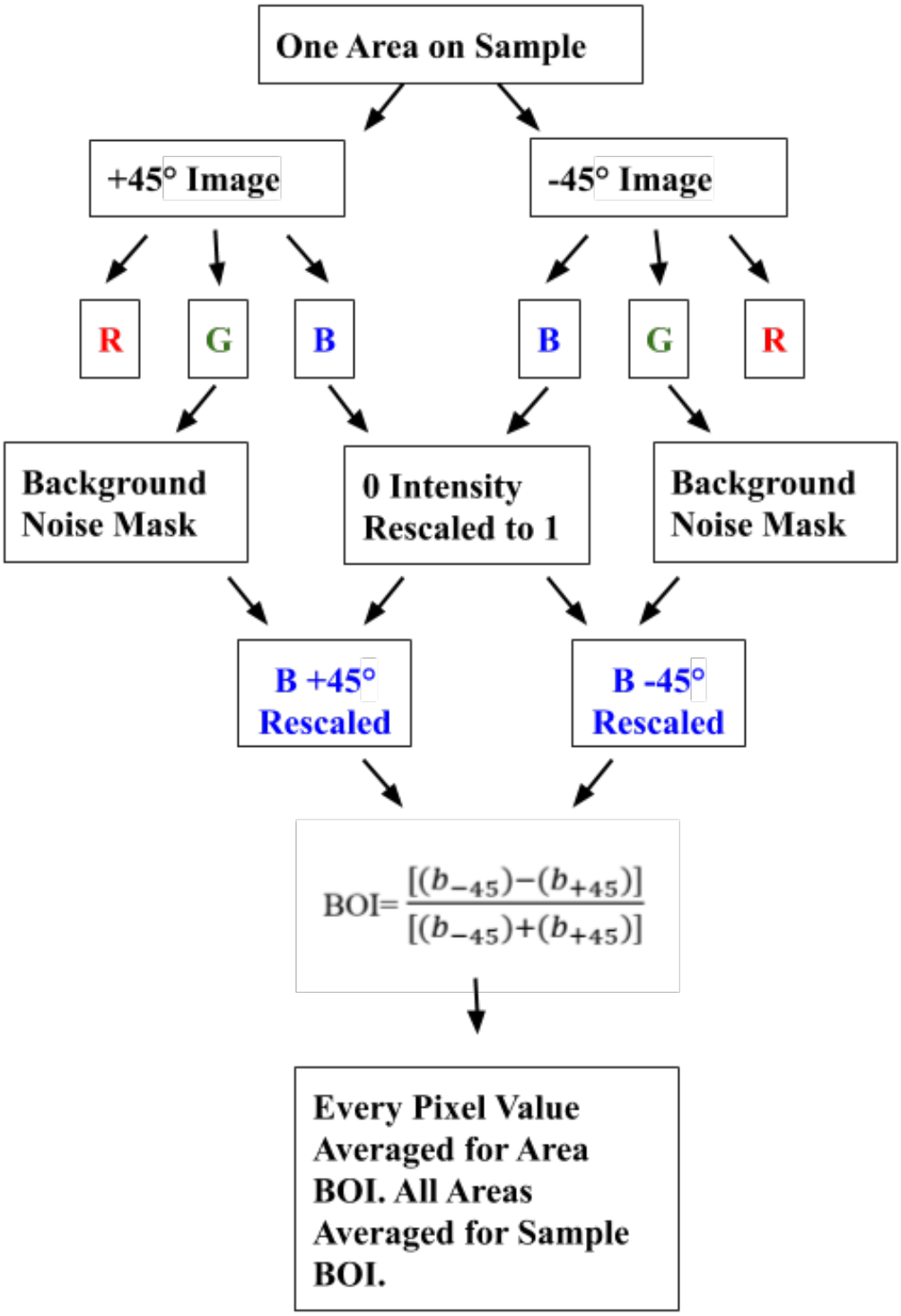

Figure 8: Image Processing Flow Chart

3.2: Scanning Electron Microscopy (SEM)

The polarized light microscopy (PLM) imaging setup cannot resolve individual fibers within the film and therefore other imaging data are needed to show that BOI directly relates to fibril orientation. SEM is a readily available methodology on campus and uses electromagnets to direct and propel electrons to create high resolution images down to the 10 nm scale. This works due to electrons having mass, unlike photons, and thereby a smaller DeBroglie wavelength, which allows imaging past the Abbe's diffraction limit of roughly 250 nm. This is necessary as CNF from the University of Maine have widths around 20-50 nm. The electrons that reflect off the sample are collected as an intensity value off every X/Y coordinate, scanning across the sample. These intensity values and coordinates are used to create an image thereby replicating images normally seen with light. This results in damaging the sample where imaged, since high energy electrons are tearing into the sample at high speeds. The cost and damaging effects of SEM caused this methodology to be used as supporting data. Unlike BOI, where the effects of orientation on light are being seen, SEM directly elucidates the fibrils themselves which allows accurate measurements of orientation and directionality. The specific microscope used in this research was a Zeiss NVision 40. SEM micrographs were obtained at 3 KV and 1000X magnification. These images were analyzed using a FIJI plugin known as OrientationJ. This plugin is used to characterize the dominant orientation vector direction based on evaluation of the structure tensor in a local neighborhood [27]. In order to reduce the effect of noise, a 3x3 matrix (local neighborhood) was blurred using a gaussian function to create a smoothed image. This window is also used to calculate an orientation direction for each pixel by using a Gaussian gradient to solve for the directional derivative. The directional derivatives can be used to calculate the orientation angle by comparison to a unit vector.

The structure tensor is also used to calculate a coherency value for each pixel by the OrientationJ plugin. A pixel with coherency of 1 represents an oriented local area, where 0 is an isotropic area. In this method, the coherency data is used as weight on the directional derivatives to recreate a directionality polar plot (**Figure 17)**.

3.3: GLCM and Alignment Values from Fast Fourier Transform

Two other image analysis methodologies performed on birefringence images to determine fibril orientation were found in the literature and applied to the samples produced by the vacuum filtration methodology images [28, 29]. A texture analysis using GLCM data was collected by running the Texture Analyzer plugin created by Julio E. Cabrera available on the NIH website [29, 30]. By taking a color channel of the birefringent images, such as blue, the image could be converted to a gray scale image with gray pixel intensity representing blue color intensity. Fibrils running in the same direction should have similar color intensities, which can be seen in the unoriented birefringent images shown later on in results, such as **Figure 12**. Using a 4 by 4 pixel square window scanning across the image, the co-occurrence correlation value is calculated using the gray-scale intensity values [30]. The scanning directions selected were 0° and 90° where 90° was in the direction the sample was stretched. In images of defined fibrils running in the same direction, a higher correlation value was expected than unoriented samples. For each sample, the imaged areas correlation values were averaged, and a standard deviation was calculated. Oriented samples had correlation values ranging from $2.5x10^{-4}$ to $8.5x10^{-4}$ while unoriented samples ranged from $2x10^{-4}$ to $5x10^{-4}$. Oriented samples had much higher variability than unoriented. A Student's T-test was then performed on the oriented samples vs the unoriented sample populations produced from vacuum drying. A P value of 0.0006

was found for the groups being different due to random variation, with oriented samples having higher correlation values. While this data supports that more oriented samples have higher correlation between gray pixel intensity, it gives no information about orientation direction in comparison to stretch direction as it is still a PLM birefringence image. This means we are not directly elucidating fiber structure, instead the gray intensity values represent peak photon retardation of which is related to orientation but is not fibril orientation. Individual samples also could not pass T-Tests with the average correlation and standard deviations from the other group. Two oriented samples and two unoriented samples both failed T-tests when not grouped with the statistically significant samples. Individual areas on unoriented samples were reaching the same peaks of oriented samples even if they were a lower BOI area. The goal was to confidently tell if an individual sample was oriented or not and use the correlation value as a degree of orientation, which caused the abandonment of this image analysis methodology.

The other methodology found was calculating an alignment value from Fast Fourier Transforms (FFT) of a color channel. The FFT was performed on the blue color channel of a birefringent image directly in FIJI which has the option by default. It transforms the image into its component frequencies [31]. This means if the image is dominated by oriented fibrils, the FFT would pick up on the higher spatial frequency of the fibrils and have more intense gray pixel values along that frequency within the produced power spectrum. A plugin called Radial Profile Extended by Phillipe Carl was used [27]. This plugin averaged the intensity along a straight line at each angle, calculating 360 intensity values at angles from 0° to 359°. In fibril analysis, a standardized methodology known as alignment value was developed using FFT images [28, 29]. This involves summing the 45 and 225 angles (stretch direction) intensity values in comparison to the 135 and 315 angles

(orthogonal to stretch direction). A ratio is then produced by dividing stretch direction by the orthogonal direction. The higher the value, the more anisotropic the frequency is in the stretch direction compared to the non-stretch direction which is indicative of orientation. This did not create statistically significant results with our samples which in retrospect makes logical sense. The images used in studies published with this methodology had well defined fibrils over dark backgrounds, whereas the single channel BOI images shown later on in **Figure 13** and **Figure 15** do not have a defined fibril direction. This is due to the fibrils being on a smaller scale than the image taken, and what look like individual fibers in some cases are actually fibril bundles. Oriented samples look like a field of color due to this scale issue and no fibril orientation can be elucidated. This analysis methodology was abandoned due to this but could still be used in the future for higher resolution SEM images of films.

CHAPTER 4: RESULTS

4.1: Vacuum Filtration Compared to Substrate Drying

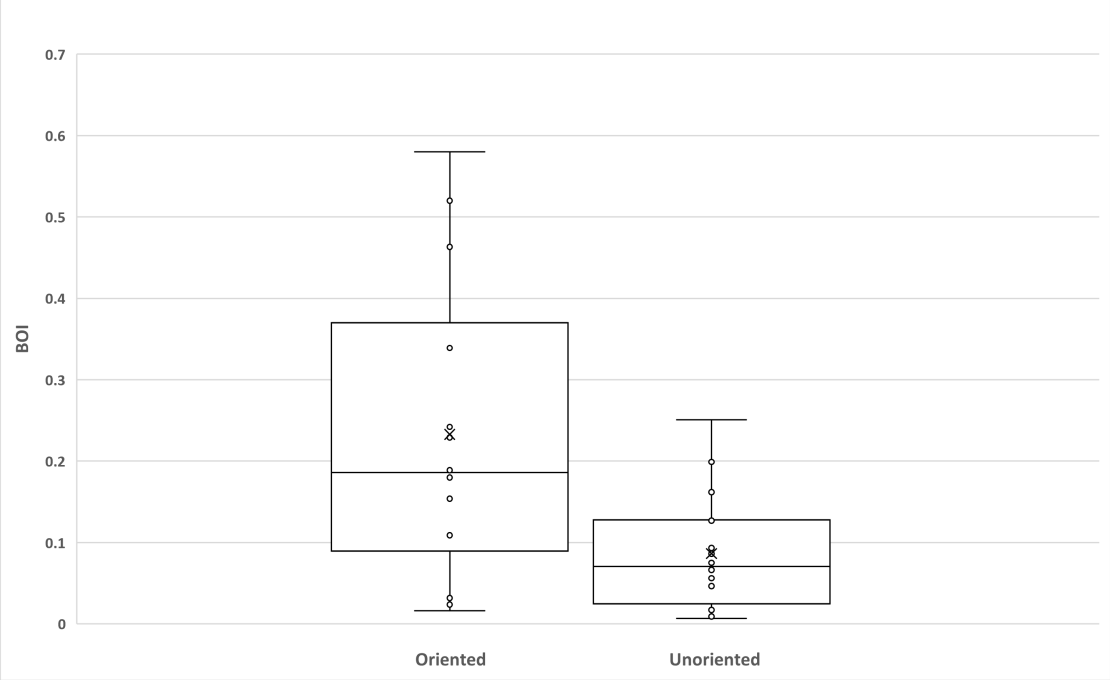

Figure 9: Absolute Value of BOIs From Oriented and Unoriented Samples Using Vacuum Filtration

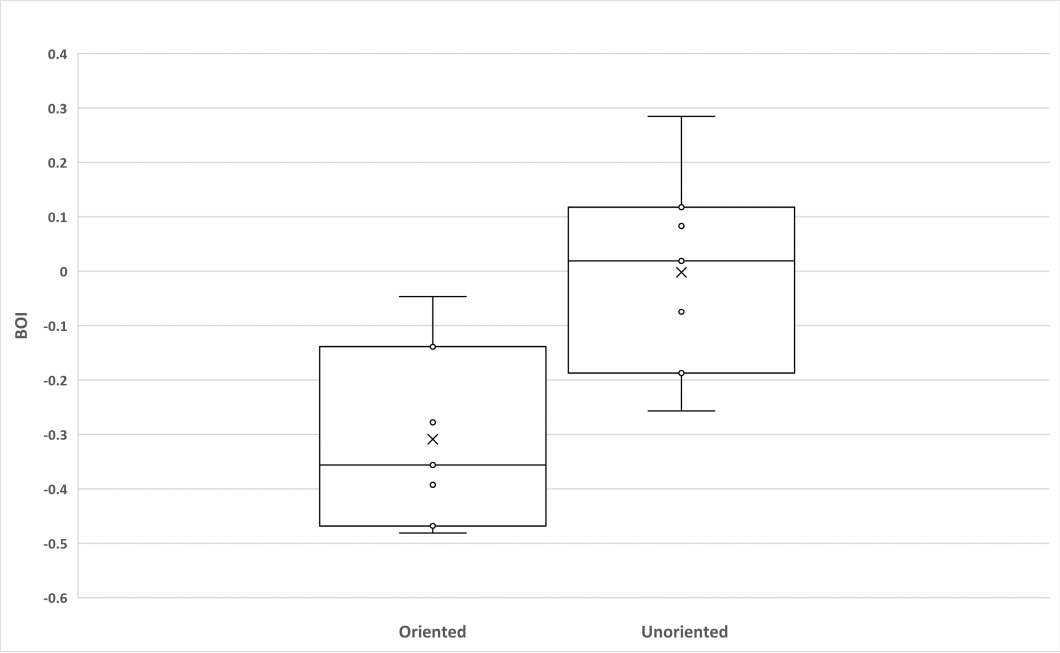

Figure 10: NON-Absolute Value BOIs of Oriented and Unoriented Samples Using Substrate Drying

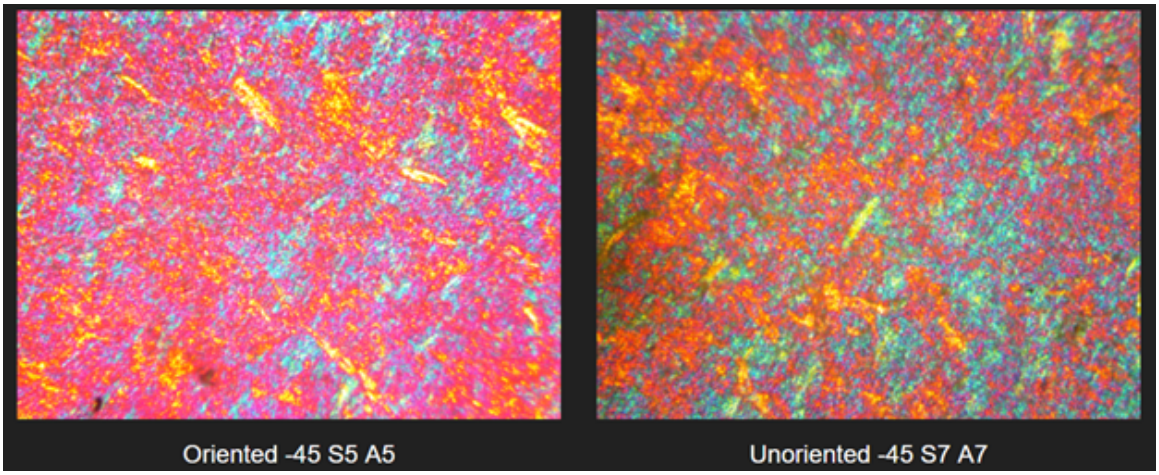

Figure 11: Side by Side Comparison of Birefringence Images of Films Made Using Vacuum Filtration

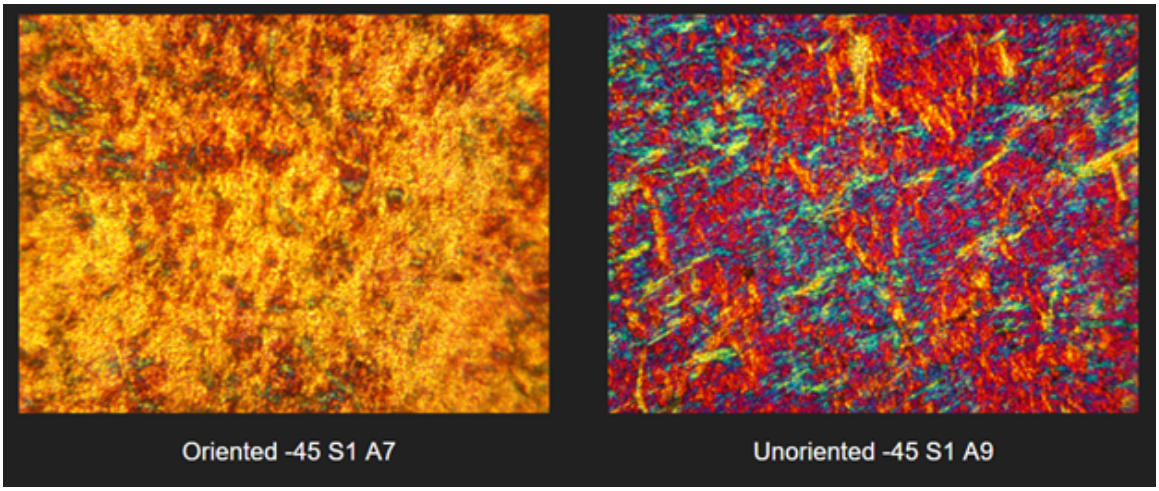

Figure 12: Side by Side Comparison of Birefringence Images of Films Made Using Substrate Drying

Figures 9 and **10** are box and whisker plots of BOI values as compared between oriented and unoriented samples using two different orientation methodologies. The circles are individual sample BOIs that are within the second quartile range and the X is the median sample's BOI. An important thing to note is that **Figure 9** has the absolute values of the film BOI rather than just their values. Vacuum Filtration produces films with varying BOIs within the same sample which causes area averaging to lead to an average sample BOI of

zero. To compare oriented and unoriented samples the absolute value of the birefringent index was taken before area averaging. Oriented vacuum dried samples have high variability as compared to unoriented samples and, on average, are only skewed to higher BOIs rather than being an entirely different population distribution. **Figure 11** shows the side-by-side similarities between the oriented and unoriented samples produced by this sample type. For the samples made using rubber substrate machine stretching there was no need to take the absolute value in order to compare sample populations shown in **Figure 10**. The samples made in the oriented method were consistently negatively birefringent across the whole sample area with an average value of -0.318, which this negative birefringence is expected for CNF [29]. Unoriented samples followed a gaussian like distribution around zero. **Figure 12** is a side by comparison of the two sample types and a stark color shift can be seen rather than the minor one in **Figure 11.**

4.2: Results of Final Methodology with Weight Tuning

Due to the success of the substrate drying, tests using the improved final methodology were done. This methodology allows control over the force applied upon the sample which allows for a tuning of orientation by tuning the weight. The amount of force applied vertically to stretch the wet sample was quantified by measuring the maximum force required to fully stretch the band without breaking the sample. For each weight applied, the BOI was calculated. The results of force optimization experiments indicate that the average BOI increases when more force is applied. However, when the force exceeded from 10.2 N, the sample became disintegrated, and the film was not formed. **Table 1** indicates the amount of force applied to the samples before drying and the average BOI value pertaining to each force.

Table 1: The Average BOI Achieved by Applying Different Forces to one end of Pure CNF Samples

Weight (lb.)	Force(N)	Average BOI
0	0	-0.16
1	4.4	-0.24
2	8.8	-0.57
2.3	10.2	-0.80
2.4	11.1	Sample broke

Figure 13 shows the PLM images captured at -45° and +45° for unstretched and stretched samples. Unstretched samples did not show a significant color change when rotated 90° while the stretched CNF films showed a significant color transition from yellow to blue between indicating the change in fiber orientation between angles. The BOI map, shown in row 3 of **Figure 13**, is produced by a macro using **Equation 2**, and the figure indicates that the map changed from a gray image for the unstretched sample to a black dominant image for the stretched sample, where +1 BOI represents a full white image and -1 BOI represents an entirely black image. This demonstrates the final methodology is causing a significant change in sample BOI between stretched and unstretched.

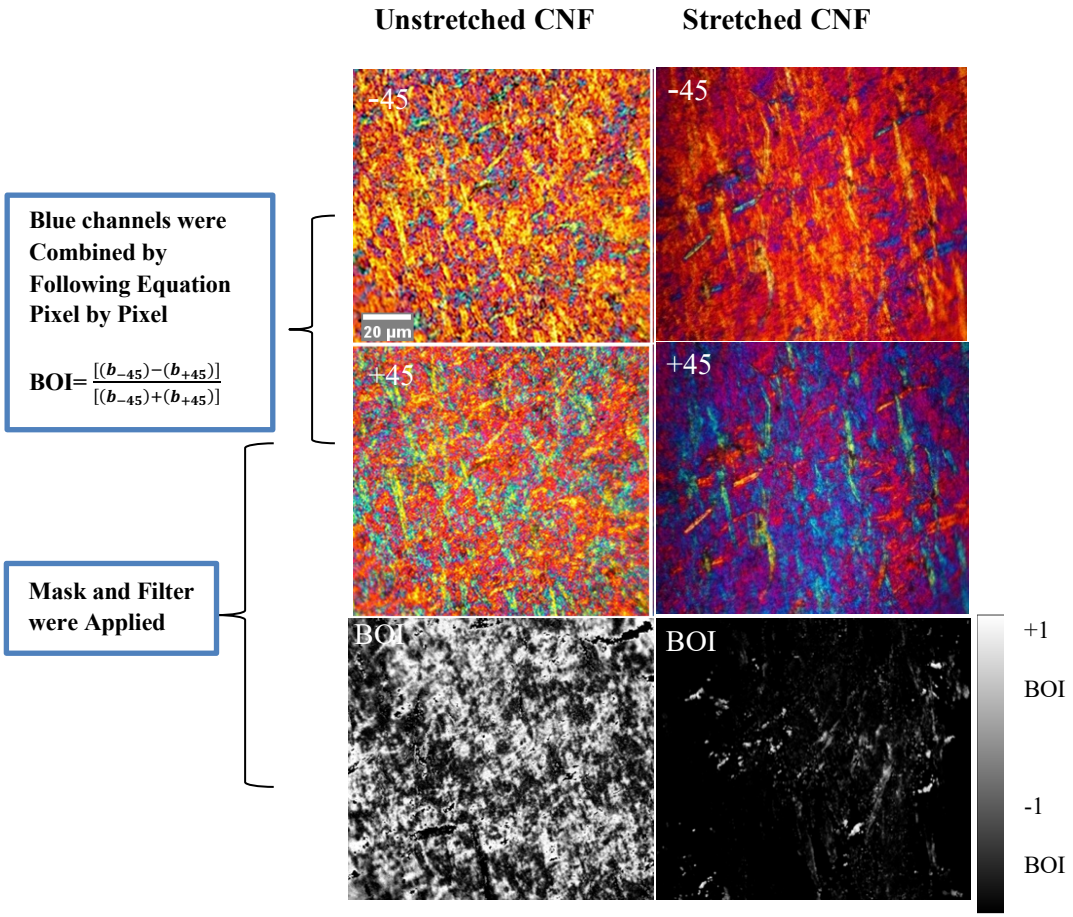

Figure 13: Polarized light image of unstretched and stretched samples showing the color transition when samples were rotated between -45° and +45°

The histograms of BOI value calculated by FIJI software are represented in **Figure 14**. This includes every sample made using the final methodology. The frequency in **Figure 14** represents the number of pixels, normalized to a 0.001-1.0 scale in logarithmic form,

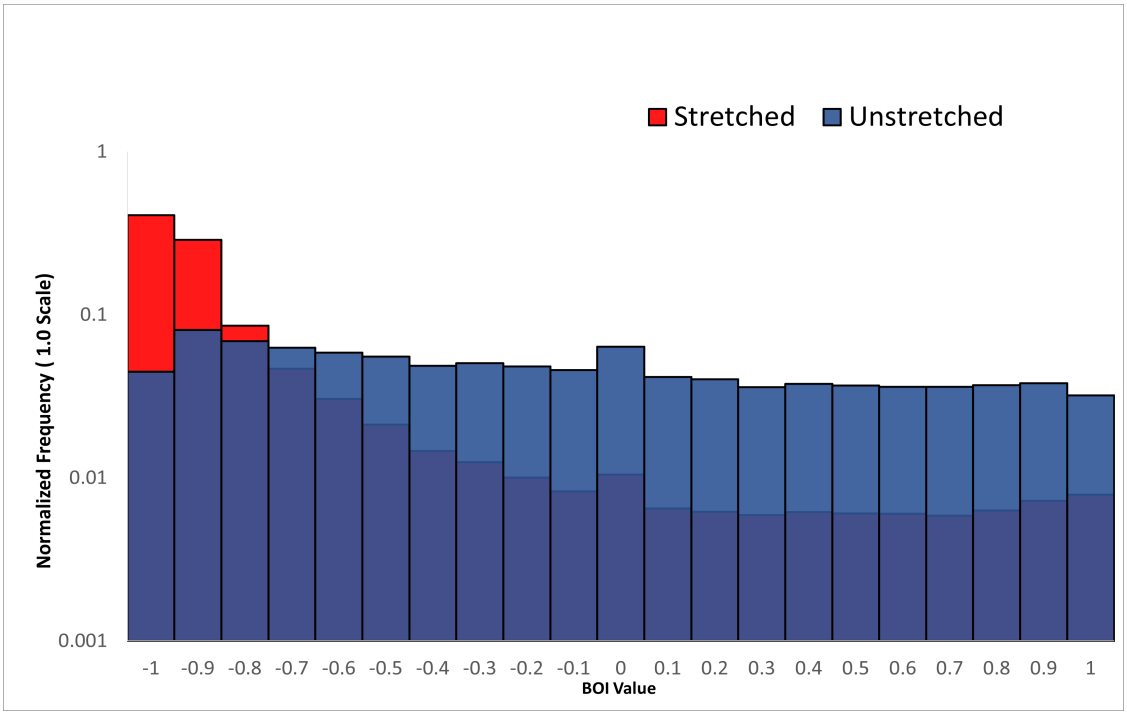

Figure 14: BOI vs Normalized Frequency of Stretched Pure CNF and Unstretched Pure CNF

that fell into their respective bins shown on the x-axis from all samples. This allows for a visual comparison between the BOI distribution of samples. According to **Figure 14**, the stretched CNF Samples are skewed to -1 BOI values, while unstretched samples do not have a similar skewness level for BOI values, suggesting a significant increase in orientation for stretched CNF samples.

4.3: Results of Hydroxyapatite Addition (HA)

For the advantages of this methodology to be demonstrated, samples were made with HA following the procedure as described in the methodology section. These were compared to stretched samples using the same methods as comparing stretched and unstretched samples. The goal is to demonstrate that adding nanoparticles for substrate modifications will not affect CNF orientation and that CNF/HA samples will be similar to stretched CNF samples.

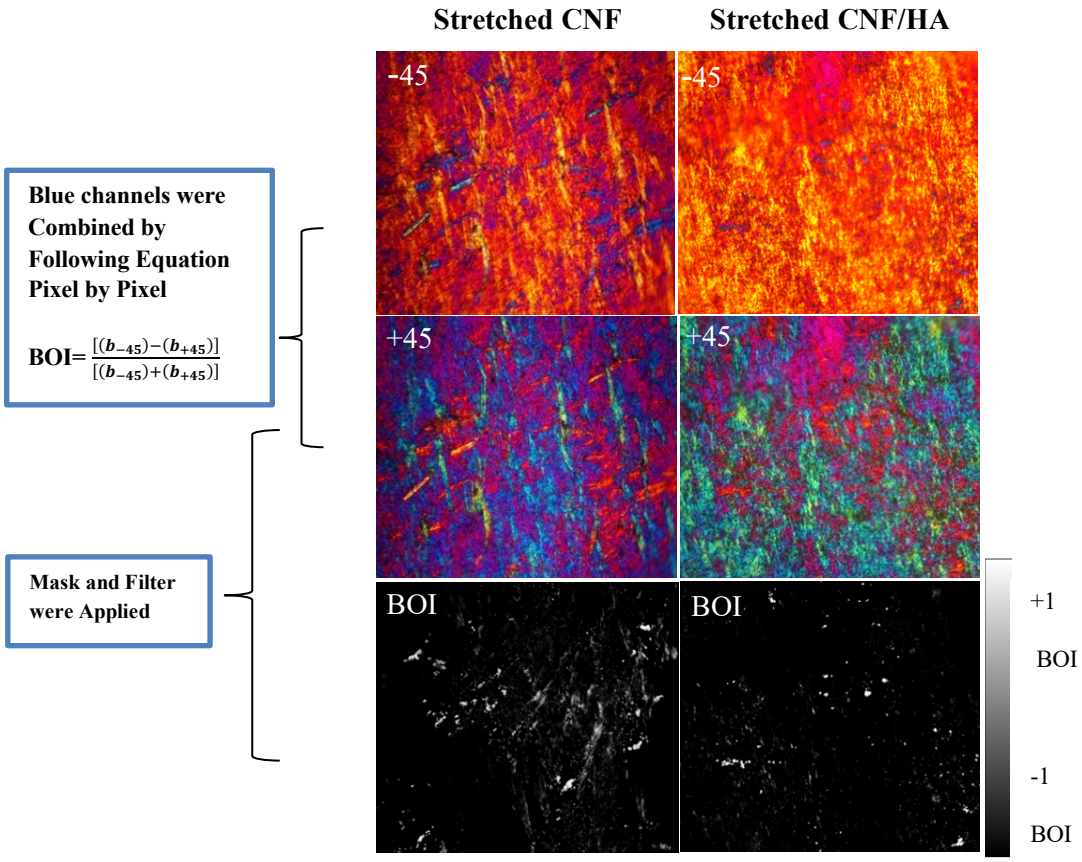

Figure 15: Polarized Light Image of Stretched and Stretched CNF/HA Samples Showing the Color Transition When Samples Were Rotated Between -45° and +45°

Figure 15 shows the PLM images captured at -45° and +45° for stretched and unstretched CNF/HA samples. CNF/HA samples do not seem to have significant differences from stretched samples and their BOI maps have a similar visual appearance. This is further supported by **Figure 16**, which was created using the same processing as **Figure 14**. The stretched CNF/HA sample follows a similar BOI frequency trend to the pure stretched CNF sample demonstrating that adding HA did not interfere with fiber orientation.

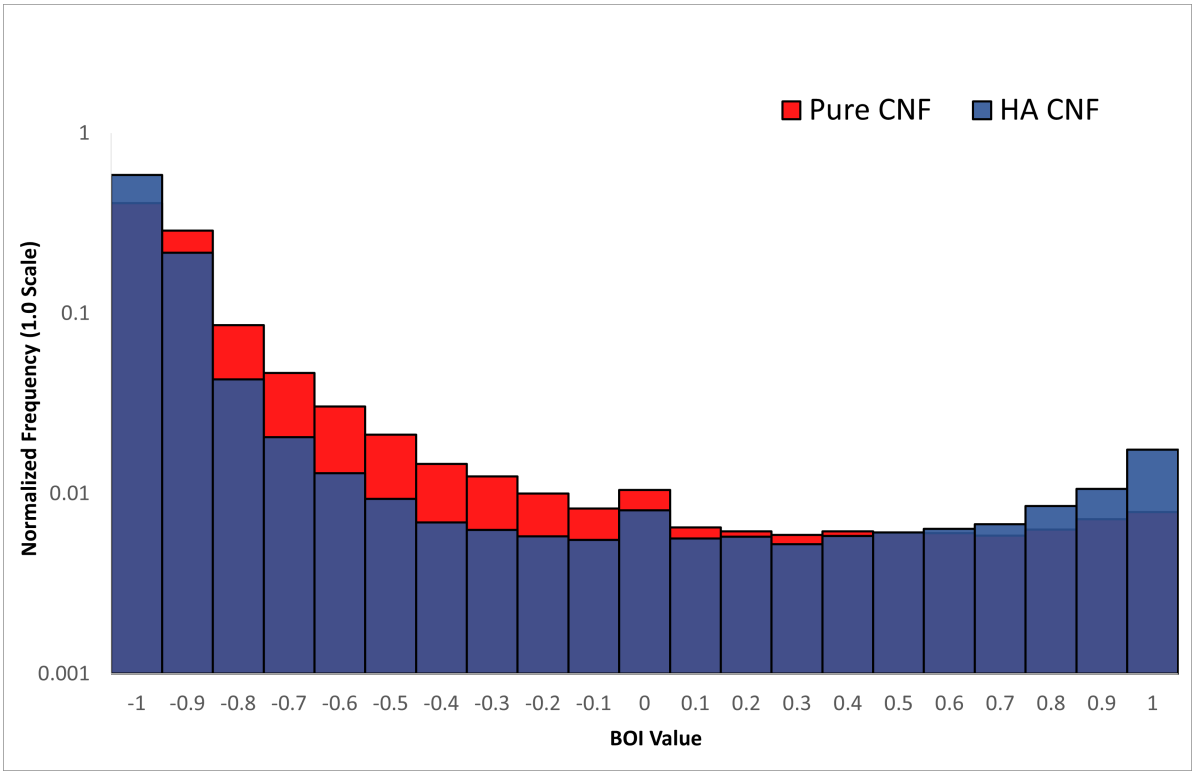

Figure 16: BOI vs Normalized Frequency of Stretched Pure CNF and Stretched CNF/HA

4.4: Results of SEM

In order to confirm that the BOIs calculated from PLM images are caused by fiber orientation in the stretch direction, SEM images were taken of the samples. **Figure 17A** represents the color-coded image of each sample created by OrientationJ plugin. The hue-saturation-brightness (HSB) color maps of unstretched and stretched samples, illustrate a transition of color from a map with no dominant color for unstretched sample to a purplish red map for stretched pure CNF and CNF/HA samples. The fiber orientation towards the stretch direction is visible in color map of stretched samples shown in **Figure 17A**.

Figure 17B depicts the orientation distribution of fibers on the surface of films. The polar plot represents the orientation angle versus normalized frequency for each group of samples. The unstretched sample polar plot indicates that there is a broad orientation distribution with no obvious preferred angle while stretched pure CNF and CNF/HA samples appeared to have a narrower orientation distribution suggesting the unilateral force application was successful in orientating films. However, due to limitations in zoom on the scanning electron microscopy setup used, it does not provide a high-resolution image of the individual fibers, so the extent of orientation and degree of orientation are approximate as each fiber is only a few pixels.

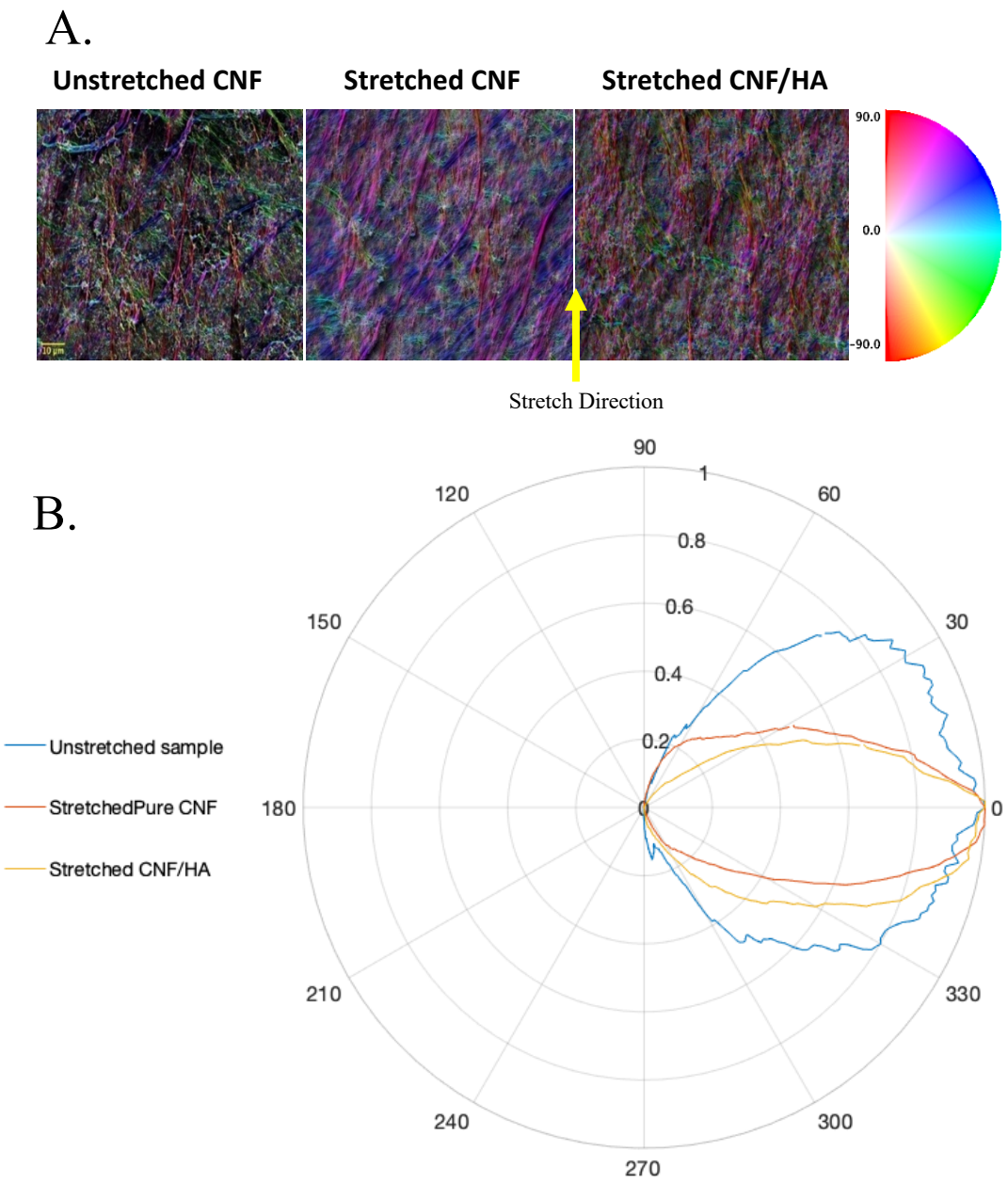

Figure 17: SEM Image Analysis Using OrientationJ Plugin for ImageJ **A)** SEM Images of Film After OrientationJ Processing, Yellow Arrow is Stretch Direction **B)** Normalized Polar Plot of Orientation Directions, 0° is Same Direction as Yellow Arrow

4.5: Results of Cell Viability Testing

Due to COVID-19, the cell culture lab was closed over the summer when most of the research was conducted. This resulted in cell research beginning the month of December in 2020. Currently, a 24-, 48-, and 72-hour MTT assay using MC3T3 cells on oriented and unoriented CNF films is underway to determine cell metabolic activity. A fluorescein diacetate (FDA) and propidium iodide (PI) stain will be conducted to determine cell viability on the two different films. Viable cells will fluoresce green where nonviable fluoresce red. These fluorescing cells can be imaged underneath a widefield fluorescence microscope and counted in FIJI. The goal after FDA/PI staining is to conduct actin cytoskeleton stains on the two different CNF film substrates to determine initial cellular integration differences.

CHAPTER 5: DISCUSSION AND FUTURE WORK

5.1: Viability and First Applications of Final Methodology

In this work, a novel method to induce fiber orientation on CNF films, regardless of HA nanoparticle addition was developed and the viability was demonstrated by **Figures 11-15** shown in the results section. The average negative BOI value was increased significantly for both stretched pure CNF and stretched CNF/HA samples as compared to other methodologies and unstretched samples. The SEM results confirmed the data received by polarized light microscopy in terms of fiber orientation and a preferred orientation angle were detected for stretched samples. The results indicate that incorporating HA in the CNF structure does not interfere with fiber orientation and film consistency. This method can be applied using other nanoparticle additives such as Titania for further investigations in the future. Highly oriented films achieved by this method are beneficial for tissue engineering and various biomedical applications. For example, Dr. Michael Mason and his research into using CNF as a bone implant biomaterial and Dr. David Neivandt's research into nerve conduits using CNF. This methodology, due to its simplicity and cost effectiveness, could also be upscaled and applied for industrial applications of CNF materials by controlled liquid injection of CNF onto rubber substrates and then mechanically stretching those substrates.

5.2: Exploration of Layered Film Birefringence Images

One observation found while researching CNF orientation is an interesting phenomenon occurring in most of the hundreds of birefringence images produced throughout this research. The reader might have caught earlier, that a non-birefringent material should have no color changing effects, and that CNF birefringence is due to polymer scale orientation. Yet, unoriented CNF samples still produce birefringent images as they still form long polymers resulting in birefringence caused by the many hydrogen bonding sites. There seems to an orthogonal layer of positive birefringent CNF in almost

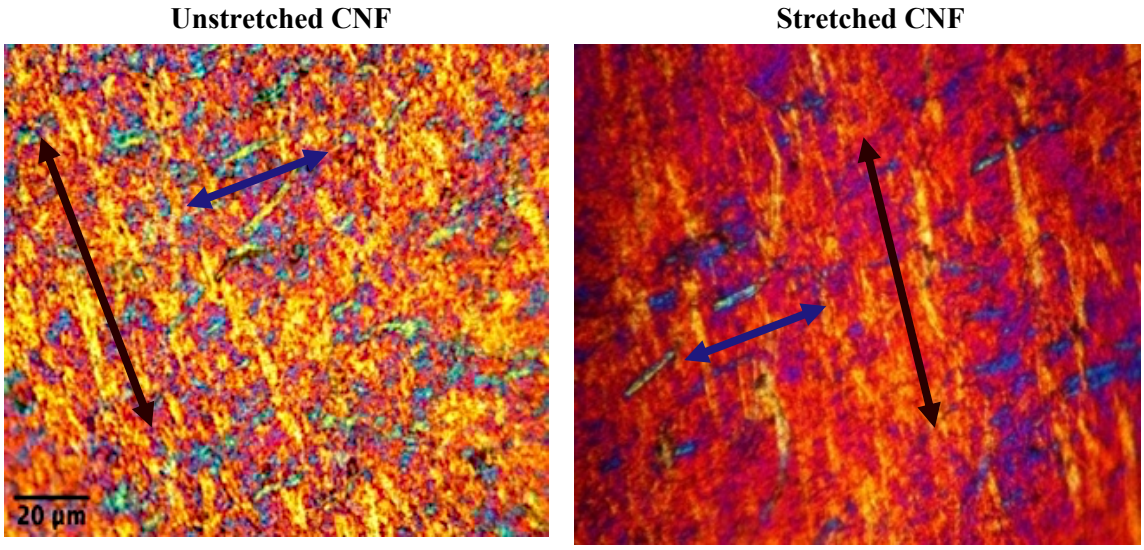

Figure 18: Orientation of Birefringent Patterns

all images of unoriented and oriented films. This can be demonstrated in **Figure 16**, using the -45° unstretched and stretched images shown in **Figure 11**. This phenomenon can also be noticed in **Figure 13**. In both images the red, negative birefringence, axis is pointed roughly vertical, slightly offset to the left. The blue, positive birefringent parts of the image seem to be running in an orthogonal direction, being slightly left to horizontal. This can also be seen when the blue/red areas flip in the +45° images. It seems that more orientated

films, eliminate this counter birefringence layer from forming, possibly due to the strain caused by the stretching preventing the preferred orthogonal orientation pattern of CNF bundles from being a lower energy state. CNF fibrils have many hydrogen bonding sites, and this directional force could be breaking orthogonal fibril hydrogen bonding preventing them from forming, thus causing the massive BOI shift. A possible future research path could involve exploring this theory more, thereby elucidating more information about CNF 3d matrix patterns.

5.3: Future Work

Now that a simple, low cost, and effective method for controlled orientation and quantification of stretched CNF films has been developed, the next steps are to determine how to best prepare samples for different cell types. This would involve creating a multitude of samples at different stretch levels and incorporating different nanoparticles, such as HA as before. These samples can now be embedded with cell cultures for actin cytoskeleton staining in order to determine if cell orientation and proliferation can be controlled by tuning the orientation of CNF films. This would further demonstrate the viability of CNF as an implantable biomaterial for medical applications where the body can slowly absorb and replace the CNF over time, such as nerve repair conduits or bone support implants after breaks. If these results prove successful the next steps could involve researching if CNF orientation can affect rates of tissue replacement allowing an easy, inexpensive, and applicable way to modify reabsorption/replacement of an implant. This research may also be applied in areas where the anisotropic properties of CNF strength need to be tuned to reach certain values, such as tensile strength or young's modulus, for

using CNF as a replacement biopolymer, where its inherent biodegradability would reduce plastic waste in our environments.

REFERENCES

[1] S. Solomon, G.-K. Plattner, R. Knutti, and P. Friedlingstein, “Irreversible climate change due to carbon dioxide emissions,” *Proc. Natl. Acad. Sci.*, vol. 106, no. 6, pp. 1704–1709, Feb. 2009, doi: 10.1073/PNAS.0812721106.

[2] D. Horton, “Advances in Carbohydrate Chemistry and Biochemistry,” vol. 64, D. Horton, Ed. Academic Press, 2010, pp. xi–xiii.

[3] K. Zhang, A. Barhoum, C. Xiaoqing, H. Li, and P. Samyn, “Cellulose Nanofibers: Fabrication and Surface Functionalization Techniques,” in *Handbook of Nanofibers*, 2019.

[4] “Nanocellulose - The Process Development Center - University of Maine.” umaine.edu/pdc/nanocellulose/.

[5] Listo, Ariel, "Past, Present and Future of Maine's Pulp and Paper Industry" (2018). Electronic Theses and Dissertations. 2903. https://digitalcommons.library.umaine.edu/etd/2903

[6] Lin, Ning, and Alain Dufresne. “Nanocellulose in Biomedicine: Current Status and Future Prospect.” *European Polymer Journal*, vol. 59, 1 Aug. 2014, pp. 302–325., doi:10.1016/j.eurpolymj.2014.07.025.

[7] Sultan, Sahar, et al. “3D Printing of Nano-Cellulosic Biomaterials for Medical Applications.” Current Opinion in Biomedical Engineering, vol. 2, 15 June 2017, pp. 29–34., doi:10.1016/j.cobme.2017.06.002.

[8] Ghaderi, Moein, et al. “All-Cellulose Nanocomposite Film Made from Bagasse Cellulose Nanofibers for Food Packaging Application.” *Carbohydrate Polymers*, vol. 104, 10 Jan. 2014, pp. 59–65., doi:10.1016/j.carbpol.2014.01.013.

[9] Ahne, Joerg, et al. “Electrospun Cellulose Acetate Nanofibers for Airborne Nanoparticle Filtration.” Textile Research Journal, vol. 89, no. 15, 28 Oct. 2018, pp. 3137–3149., doi:10.1177/0040517518807440.

[10] CryoLife, “Mitral Heart Valve with Standard Sewing Ring.” https://www.cryolife.com/products/on-x-heart-valves/mitral-heart-valve-with-standard-sewing-ring/.

[11] S. J. P. Callens, R. J. C. Uyttendaele, L. E. Fratila-Apachitei, and A. A. Zadpoor, “Substrate curvature as a cue to guide spatiotemporal cell and tissue organization,” *Biomaterials*, vol. 232, no. December 2019, p. 119739, 2020, doi: 10.1016/j.biomaterials.2019.119739.

[12] C. A. Bashur, L. A. Dahlgren, and A. S. Goldstein, “Effect of fiber diameter and orientation on fibroblast morphology and proliferation on electrospun poly(d,l-lactic-co-glycolic acid) meshes,” *Biomaterials*, vol. 27, no. 33, pp. 5681–5688, 2006, doi: 10.1016/j.biomaterials.2006.07.005.

[13] C. Y. Xu, R. Inai, M. Kotaki, and S. Ramakrishna, “Aligned biodegradable nanofibrous structure: A potential scaffold for blood vessel engineering,” *Biomaterials*, vol. 25, no. 5, pp. 877–886, 2004, doi: 10.1016/S0142-9612(03)00593-3.

[14] A. I. Teixeira, G. A. Abrams, P. J. Bertics, C. J. Murphy, and P. F. Nealey, “Epithelial contact guidance on well-defined micro- and nanostructured substrates,” *J. Cell Sci.*, vol. 116, no. 10, pp. 1881–1892, 2003, doi: 10.1242/jcs.00383.

[15] S. Ghasemi, P. Rahimzadeh-Bajgiran, M. Tajvidi, and S. M. Shaler, “Birefringence-based orientation mapping of cellulose nanofibrils in thin films,” *Cellulose*, 2020, doi: 10.1007/s10570-019-02821-2.

[16] Lee MJ, Sohn SK, Kim KT, Kim CH, Ahn HB, Rho MS, Jeong MH, Sun SK. Effect of hydroxyapatite on bone integration in a rabbit tibial defect model. Clin Orthop Surg. 2010 Jun;2(2):90-7. doi: 10.4055/cios.2010.2.2.90.

[17] M. Chesley, R. Kennard, S. Roozbahani, S. M. Kim, K. Kukk, and M. Mason, “One-step hydrothermal synthesis with in situ milling of biologically relevant hydroxyapatite,” *Mater. Sci. Eng. C*, vol. 113, 2020, doi: 10.1016/j.msec.2020.110962.

[18] H. C. Kim, J. W. Kim, L. Zhai, and J. Kim, “Strong and tough long cellulose fibers made by aligning cellulose nanofibers under magnetic and electric fields,” *Cellulose*, 2019, doi: 10.1007/s10570-019-02496-9.

[19] Mittal, N. *et al.* Multiscale Control of Nanocellulose Assembly: Transferring Remarkable Nanoscale Fibril Mechanics to Macroscale Fibers. *ACS Nano* **12**, 6378–6388 (2018).

[20] L. Larsen, L. D. Griffin, D. GRäßel, O. W. Witte, and H. Axer, "Polarized light imaging of white matter architecture," *Microsc. Res. Tech.*, vol. 70, no. 10, pp. 851–863, 2007, doi: 10.1002/jemt.20488.

[21] "'Anisotropy and Birefringence.' Birefringence, University of California, Berkeley, microscopy.berkeley.edu/courses/tlm/plm/birefr.html."

[22] "'Lecture Notes - Optics 3: Double Refraction, Polarized Light.' Geosciences, Smith College, www.science.smith.edu/geosciences/min_jb/Optics/Optics-3.pdf."

[23] K. M. O. Håkansson, F. Lundell, L. Prahl-Wittberg, and L. D. Söderberg, "Nanofibril Alignment in Flow Focusing: Measurements and Calculations," *J. Phys. Chem. B*, vol. 120, no. 27, pp. 6674–6686, Jul. 2016, doi: 10.1021/acs.jpcb.6b02972.

[24] D. G. Castner and B. D. Ratner, "Biomedical surface science: Foundations to frontiers," *Surf. Sci.*, 2002, doi: 10.1016/S0039-6028(01)01587-4.

[25] B. E. Sørensen, "A revised Michel-Lévy interference colour chart based on first-principles calculations," *Eur. J. Mineral.*, 2013, doi: 10.1127/0935-1221/2013/0025-2252.

[26] Philippa J. M. Jian Guo Liu, *Image processing and GIS for remote Sensing Techniques and applications*. 2016.

[27] T. D. Clemons *et al.*, "Coherency image analysis to quantify collagen architecture: Implications in scar assessment," *RSC Adv.*, 2018, doi: 10.1039/c7ra12693j.

[28] E. C. Rentchler, K. L. Gant, R. Drapkin, M. Patankar, and P. J. Campagnola, "Imaging collagen alterations in STICs and high grade ovarian cancers in the fallopian tubes by second harmonic generation microscopy," *Cancers (Basel).*, vol. 11, no. 11, 2019, doi: 10.3390/cancers11111805.

[29] B. de C. Vidal and M. L. S. Mello, “Optical anisotropy of collagen fibers of rat calcaneal tendons: An approach to spatially resolved supramolecular organization,” *Acta Histochem.*, vol. 112, no. 1, pp. 53–61, 2010, doi: 10.1016/j.acthis.2008.07.005.

[30] M. Hall-Beyer, “Glcm Texture: a Tutorial,” *Univ. Calgary*, vol. 3.0, no. March, pp. 1–75, 2017.

[31] Schindelin, J.; Arganda-Carreras, I. & Frise, E. et al. (2012), "Fiji: an open-source platform for biological-image analysis", *Nature methods* 9(7): 676-682, PMID 22743772, doi:10.1038/nmeth.2019

AUTHOR'S BIOGRAPHY

Joshua Hamilton was born in Dover Foxcroft, Maine, on December 18th, 1998. He was raised in Alton, Maine, and graduated from Old Town High School in 2017. During his four years at the University of Maine, Josh was enrolled as part of the Honors College, majored in Bioengineering, and has a minor in Nanotechnology. In his Junior year he was invited and joined as part of the national engineering honors society, Tau Beta Pi and was elected Vice President of the organization the following semester.

Upon his graduation in May 2021, Josh plans to pursue further education with the hopes of obtaining a PhD. His dream is to become a professor, teaching the next generation of scientists and engineers whilst researching solutions to diseases that plague society in hopes of easing the suffering of others. He dreams others would not have to experience loss of loved ones like he has at the ages of 18 and 19.